Journal of Imaging Science and Technology® 64(2): 020501-1–020501-10, 2020.

A Pilot Study on Electroencephalogram-based Evaluation of Visually Induced Motion Sickness

Ran Liu
College of Computer Science, Chongqing University, Chongqing, China
Schepens Eye Research Institute, Massachusetts Eye and Ear, Department of Ophthalmology, Harvard Medical School, Boston, MA, USA
School of Microelectronics and Communication Engineering, Chongqing University, Chongqing, China

Miao Xu
College of Information Science and Engineering, Shanxi Agricultural University, Taigu County, Jinzhong City, Shanxi Province, China

Yanzhen Zhang
School of Microelectronics and Communication Engineering, Chongqing University, Chongqing, China

Eli Peli and Alex D. Hwang
Schepens Eye Research Institute, Massachusetts Eye and Ear, Department of Ophthalmology, Harvard Medical School, Boston, MA, USA
E-mail: alex_hwang@meei.harvard.edu

Abstract. *The most prominent problem in virtual reality (VR) technology is that users may experience motion-sickness-like symptoms when they immerse into a VR environment. These symptoms are recognized as visually induced motion sickness (VIMS) or virtual reality motion sickness. The objectives of this study were to investigate the association between the electroencephalogram (EEG) and subjectively rated VIMS level (VIMSL) and find EEG markers for VIMS evaluation. A VR-based vehicle-driving simulator was used to induce VIMS symptoms, and a wearable EEG device with four electrodes (the Muse) was used to collect EEG data. The results suggest that individual tolerance, susceptibility, and recoverability to VIMS varied largely among subjects; the following markers were shown to be significantly different from no-VIMS and VIMS states ($P < 0.05$): (1) means of gravity frequency (GF) for theta@FP1, alpha@TP9, alpha@FP2, alpha@TP10, and beta@FP1; (2) standard deviation of GF for alpha@TP9, alpha@FP1, alpha@FP2, alpha@TP10, and alpha@(FP2–FP1); (3) standard deviation of power spectral entropy for FP1; (4) means of Kolmogorov complexity (KC) for TP9, FP1, and FP2. These results also demonstrate that it is feasible to perform VIMS evaluation using an EEG device with a few electrodes.*

[DOI: 10.2352/J.ImagingSci.Technol.2020.64.2.020501]

1. INTRODUCTION

Virtual reality (VR) technology has advanced significantly in recent years. Many new devices have been introduced to create games, movies, and other immersive experiences, suggesting that they are on their way to become mass-market products [1]. However, *visually induced motion sickness* (VIMS, also called *virtual reality motion sickness*) may occur when a person immerses into the VR environment [2–5]. VIMS is a motion-sickness-like disorder often occurring to a person exposed to an environment where the visual and proprioceptive motions are conflicting [6, 7]. A person with VIMS suffers from headaches, stomach awareness, nausea, disorientation, sweating, fatigue, and even vomiting [2, 4, 6, 8], which raises safety and health concerns for current VR platforms [2, 9]. Therefore, VIMS is considered a major hurdle for wide acceptance of VR applications.

To investigate any VIMS reduction methods, it is necessary to have tools to evaluate VIMS efficiently and effectively. The simulator sickness questionnaire (SSQ) [4, 10] has been widely used to measure the amount of VIMS experienced during VR exposure. However, this subjective evaluation method has some disadvantages: it is usually performed before and after a VIMS experiment, and due to the large length of the questionnaire, it cannot be done in real time, hence cannot describe the changes of VIMS during the exposure. As a result, it is difficult to detect the emergence of VIMS, or get the details of VIMS development by using this method. Simpler versions of the quick VIMS rating scheme were also introduced for pseudo-real-time VIMS measure [2, 11]; but they depend on subjective response, which makes the evaluation susceptible to individuals' bias. To overcome the limitations of subjective VIMS measures, objective VIMS evaluation methods based on various physiological signals, such as electrogastrogram [12], electrocardiogram [13], salivary cortisol level [4, 14, 15], blood pressure [16], pulse rate [16], electroencephalogram (EEG) [9, 17, 18], postural sway [19], electrooculogram (EOG) [20, 21], and head

Received Mar. 4, 2019; accepted for publication Nov. 9, 2019; published online Jan. 31, 2020. Associate Editor: Chaker Larabi.
1062-3701/2020/64(2)/020501/10/$25.00

movement [20], were tested. Such physiological signals can be measured continuously and precisely.

Different physiological signals are associated with different VIMS theories. For example, the EEG signal is usually related to the *sensory conflict theory* [12, 22]. The sensory conflict theory is that situations that provoke VIMS can be characterized by a condition of *sensory rearrangement* [22], in which the motion signals transmitted by the visual and vestibular system (or maybe other proprioceptive systems) are mismatched with one another, or different from what is expected from previous experience [19, 22, 23]. Many researchers measured EEG in motion sickness studies based on sensory conflict theory [6, 24], to test if the EEG measure can indicate the level of motion sickness objectively [9, 25–29].

Postural sway is usually related to the *postural instability theory* [30], which predicts that postural activity will differ between persons who are susceptible to VIMS and those who are not, and these differences exist between before and after the onset of subjective symptoms of motion sickness [19, 30–33]. The postural instability theory has provided objective measures (based on the *center of pressure* [19] and other postural indicators) to predict the occurrence of motion sickness.

The EOG signal is usually related to the *eye-movement theory* [20, 34]. This theory proposes that reflexive eye movements, such as the *optokinetic nystagmus* (OKN) during visual yaw rotation, provide eye-muscle afferences that ultimately stimulate the nervus vagus [20, 34]. VIMS severity is shown to be correlated with OKN frequency [20, 35] and OKN *slow phase velocity* (OKN SPV) [20, 36].

Head movement is usually related to the subjective vertical mismatch theory, which is actually a refinement of the sensory conflict theory proposing that not all sensory conflicts are provocative but only those associated with the sense of verticality [20]. This theory argued that VIMS symptoms may arise because subjects make inadvertent head movements while in circular vection. Such head movements cause pseudo-Coriolis effects, which are known to be VIMS provocative [20, 37].

According to the sensory conflict theory, the changes in EEG data could be accounted for by the signal conflict mechanisms in the brain [9, 17], which is believed to be one of the main causes of VIMS [6, 7, 9, 17, 28, 29, 38, 39]. Although the changes in EEG signal may be caused by other factors like distress, excitement, tiredness, etc., previous studies have shown that EEG signal changes are associated with the VIMS provoked in VR-based three-dimensional environment, where the symptoms are similar to the ones induced in the real world [4, 40].

Although previous studies have shown that the changes of VIMS symptoms did affect the changes of EEG signal [9, 17, 41, 42], the details from those studies were not consistent, and, in some cases, they contradicted each other. For example, Lin et al. claimed that the *power spectral density* (PSD) of the alpha and gamma bands of the EEG signals can be used as VIMS markers since the *correlations* between those PSDs and subjective VIMS rating exceed the correlations in other frequency bands in motion-sickness-related brain regions [9]. Naqvi et al. reported that the decrease in the power of the EEG alpha band can be a possible VIMS marker [41]. However, Chen et al. observed that the increases in the total power of the EEG alpha and theta bands were related to subjective VIMS scoring [17, 28].

The fundamental reason why these details varied may be due to the large variability of individual susceptibility to VIMS. It is reported that about 30% of viewers are suffering from VIMS when watching a moving scene [21]; however, the prevalence of VIMS can vary from 1% to 70% depending on the apparatus and stimuli [21]. In addition, the scoring of VIMS varies for each viewer [9, 21].

In this article, we describe yet another effort of testing the feasibility of EEG signal analysis for evaluating the subject's VIMS when engaged in a VR-based *vehicle-driving simulator* (VDS). Both subjective and objective methods were measured to evaluate VIMS. The means and standard deviations of *gravity frequency* (GF) [42, 43], *power spectral entropy* (PSE) [42], and *Kolmogorov complexity* (KC) [44, 45] were computed from EEG data to determine whether they can be used as VIMS markers. Those measures are reported to be highly correlated with visual fatigue [42] and mental fatigue [44], which may be the end results of VIMS.

Another goal of this article is to test whether similar results can be achieved with an EEG device with a small number of electrodes. Note that most previous studies collected the EEG data with full-scale clinical EEG equipment, which is usually expensive and inconvenient for the user to wear in a VR environment. To overcome these disadvantages, we used a wearable wireless EEG device, the Muse, for EEG data collection for its affordable price and convenience. This EEG device is a sparse recording device affording only four electrodes for EEG data collection. It supports wireless data transmission (via Bluetooth) and real-time processing. Note that more electrodes do not always lead to better results due to the complication of multidimensional signal noise. Furthermore, it is often difficult to detect VIMS onset in real time. Some researchers have tried to reduce the number of EEG electrodes used in EEG applications. Cai et al. [46] used three-electrode EEG data for depression detection. They argued that compared with 128 channels' EEG, their simpler test (three-electrode EEG) can make diagnosis more accessible and widespread, and researchers can perform more tests on more patients given the same amount of time and money [46]. To the best of our knowledge, no one has attempted to evaluate VIMS using an EEG device with less than five electrodes. Our subsequent experiments demonstrated that EEG recording of four electrodes are feasible to perform VIMS evaluation.

2. MATERIALS AND METHODS

2.1 *Subjects*

Normally sighted (or corrected to be normal vision) subjects of age from 20 to 40 years old were recruited from Schepens Eye Research Institute (SERI). All subjects gave their written

Table I. Subject information.

Subject	Sex	Age	Weight (kg)	Handedness	Been trained before	Health status	
						Vestibular system	Visual system
S1	M		76	Right-handed	No	Normal	Normal
S2	M		80	Right-handed	No	Normal	Normal
S3	M		77	Right-handed	No	Normal	Normal
S4	F		55	Right-handed	No	Normal	Normal
S5	F	20–40	63	Right-handed	No	Normal	Normal
S6	F		72	Right-handed	No	Normal	Normal
S7	F		93	Right-handed	No	Normal	Normal
S8	F		46	Right-handed	No	Normal	Normal

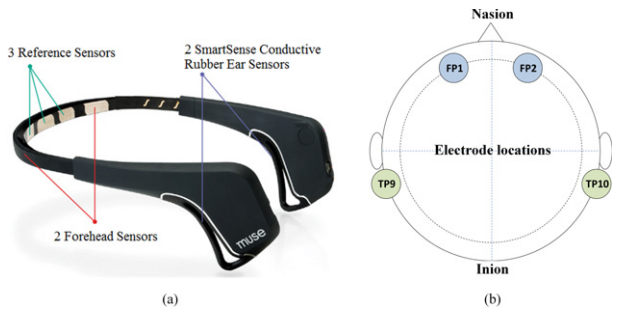

Figure 1. Muse^{TM} used for EEG recording. (a) Locations of electrodes in the Muse. (b) Top-down view of the EEG electrode positions on the subject's head.

informed consent before they participated in the study. The study was conducted in accordance with the Declaration of Helsinki. The protocol and informed consent were approved by the Institute Review Board of Schepens Eye Research Institute (16-015H). Eight subjects (three males and five females) completed the studies and their data is reported here. Table I lists information about the subjects.

2.2 *EEG Recording*

The Muse^{TM} (InteraXon Inc., Ontario Canada), shown in Figure 1(a), was used to record the EEG data continually throughout the experiment. There are four electrodes in the Muse, two are located at the frontal lobe areas (FP1 and FP2) and the other two are at the temporal lobe (TP9 and TP10) areas, as shown in Fig. 1(b) [47]. In our experiments, the analog EEG signals were sampled with 10-bit quantization at a sampling rate of 220 Hz [47]. The Muse was connected to a computer through Bluetooth; the data output was recorded and stored on the computer for post-analysis.

EEG data are usually contaminated by various artifacts, including eye blinks, muscle movements, and indoor *power-line noise* [9]. In order to remove these artifacts as much as possible, a notch filter in the Muse was adopted. The *Fast Fourier Transform* (FFT) coefficients extracted from the filtered signal by the Muse were used for the analysis. In our experiments, the FFT coefficients were used for GF and PSE computation; the filtered raw EEG data measured in microvolts was used for KC computation.

Note that many studies have shown that the dry contact EEG device (such as the Muse) performs as well as other EEG devices with wet electrodes [48–50].

2.3 *Driving Simulator for Inducing VIMS*

We used a wide field driving simulator (DE-1500, FAAC Inc. Ann Arbor, MI) to induce VIMS [47]. The VR-based driving simulator comprises a motion seat, a force feedback steering wheel, and five displays, which provides both realistic visual and proprioceptive stimulation to the subjects. All five displays are 42-inch LCD displays, covering a total horizontal field of view of 220° and vertical field of view of 63°. During the experiment, the subjects were asked to drive the simulator while wearing the Muse on their head. The same driving scenario was used for all subjects. The scenario contains a long winding road (consists of multiple winding sections) that is prone to evoke VIMS symptoms as the subjects drive the VDS through this road. Some studies [9, 18] used the EEG data collected during driving on a straight road as the baseline/control because driving on a straight road induces less motion sickness. However, it is still questionable whether the data collected within a straight-road driving can serve as a control condition because physical and emotional stimulations of driving on a winding road are clearly different from that of on a straight road. In our experiments, we also measured subjective VIMS level. Actual onset of VIMS occurred a few minutes after starting the driving on winding roads, meaning that what we measured was not just caused by "driving." In our study, VIMS was continuously measured even after the driving ended. So, we split the collected EEG data based on the VIMS states, no-VIMS (control), and VIMS (effect) to conduct within-subject and within-trial comparisons between those two states.

2.4 *Experimental Protocol*

The experiment was carried out in an air-conditioned room with a temperature of 20° C. All subjects were never exposed to the VR scenario prior to the experiment. A three-segment experimental protocol (see Figure 2) was prepared for VIMS evaluation: pre-driving, driving, and post-driving segment. Subjects were asked to complete an SSQ before and after the experiments. This pre-SSQ completion also

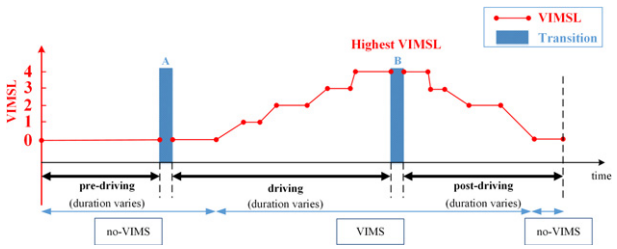

Figure 2. A typical VIMS level changes during the three-segment experimental protocol. The *x*-axis denotes the timeline and the *y*-axis denotes the measured VIMS level. The blue bars between the experimental sections indicate the transition time between getting in and out of the driving simulator.

helps the subjects to establish a more consistent VIMS rate scale by familiarizing with the VIMS symptoms before the experiment.

In the pre-driving segment, the subjects were required to remain quiet and relaxed in their favorite posture, and their baselines of physiological (EEG) state were recorded. In this segment, no-VIMS occurred for all subjects.

The driving segment comprised of driving on a long winding road. Each subject had different VIMS tolerance so actual driving duration varied from several minutes to over 30 minutes. During the driving section, the subjects verbally reported their subjective rating of *VIMS level* when they felt there was a change of VIMSL. The VIMSL can be 0 (no-VIMS), 1 (slight VIMS), 2 (moderate VIMS), 3 (severe VIMS), and 4 (very severe VIMS). We used this simple asynchronous VIMSL reporting method to obtain temporal VIMSL changes that the subjects experienced. Note that a similar temporal VIMS reporting scheme was used to measure the effect of dynamic (peripheral) visual field size change on VIMS [2]. The subjects continued to drive until they felt very uncomfortable and could not drive anymore.

After the driving stopped, the subjects left the driving simulator for post-driving measurement. In this segment, they were asked to rest to recover from the motion sickness. The duration for recovery varied between individuals.

Note that EEG data and VIMSL were recorded throughout the procedure. There were brief interruptions (e.g., for getting in and out of the driving simulator) of measurements between each segment (less than 1 minute), which are labeled as "transition" in Fig. 2. The EEG data recorded during these transition periods were excluded in our EEG data analysis.

In our experiments, each subject performed only a single trial. The data from all the subjects were used for the analysis of each potential marker. The reason why each subject did not repeat the trial is that making a subject repeat the trial may change his/her adaptation (i.e., tolerance, susceptibility, or recoverability) [51–54]. It may have an impact on the subsequent analysis of VIMSL changes. What is more, those who had ever been trained in VDS were excluded from the recruitment, as described in Table I.

2.5 *Data Processing*

The purpose of our study was to determine whether the EEG signal changes could be used as markers of a person's VIMS onset in the VR environment. We hypothesized that if VIMS was induced by the perceptual conflicts of the self-motion when interpreting the motion signals from various sensory systems in the brain, the EEG signals between no-VIMS and VIMS states should have (at least) some differences, reflecting the brain's conflicting state.

In this study, we investigated the means and standard deviations of the GF, PSE, and KC of the EEG signals as potential marker candidates for VIMS. For each subject, those potential markers of EEG signals within no-VIMS and VIMS states were computed separately and then compared within a subject. Such pairwise comparisons were done for all subjects to see if there were any significant differences between the states. The increase or decrease of the means of the candidate markers may represent the overall amount of brain activity change, while the standard deviation changes may indicate the amount of brain activity disturbance due to the VIMS. Note that the lengths of the EEG signals analyzed vary across participants (due to varied VIMS onsets and exit times). However, computing the markers within no-VIMS and VIMS states separately helps to eliminate the effects of variations of EEG signal length on the results. The remainder of this section describes the detailed methods for GF, PSE, and KC computations.

2.5.1 *Gravity Frequency*

Gravity frequency reflects the transition of EEG *power spectral density* (PSD) [42]. It allows us to see the temporal changes in brain activity within a given frequency band at each electrode location. It was computed by [42, 43]

$$GF = \frac{\sum_{f=f_1}^{f_2} \left(PSD\left(f\right) \cdot f\right)}{\sum_{f=f_1}^{f_2} PSD\left(f\right)}, \quad f_1 \le f \le f_2 \tag{1}$$

where f represents the frequency of the EEG signal, f_1 and f_2 represent the lowest and highest frequency of a given frequency band, and PSD(f) represents the power spectral density corresponding to a given EEG frequency, f.

Figure 3 shows the procedure of GF computation. Note that the PSD describes the power distribution of an EEG signal in the frequency domain for a given time period. A sliding time window of 3 minutes was empirically chosen for computing the PSD because it optimizes the trade-off between temporal resolution and computational complexity. For consistency, these raw data (FFTs) segments of 3 minutes were also used for PSE and KC computation. The PSD and GF were computed for each frequency band, i.e., delta (0–4 Hz), theta (4–8 Hz), alpha (8–12 Hz), beta (12–30 Hz), and gamma (30–50 Hz), of each electrode, i.e., FP1, FP2, TP9, and TP10.

The differences of GFs between the paired electrodes (FP2–FP1 and TP10–TP9) were alsocomputed for

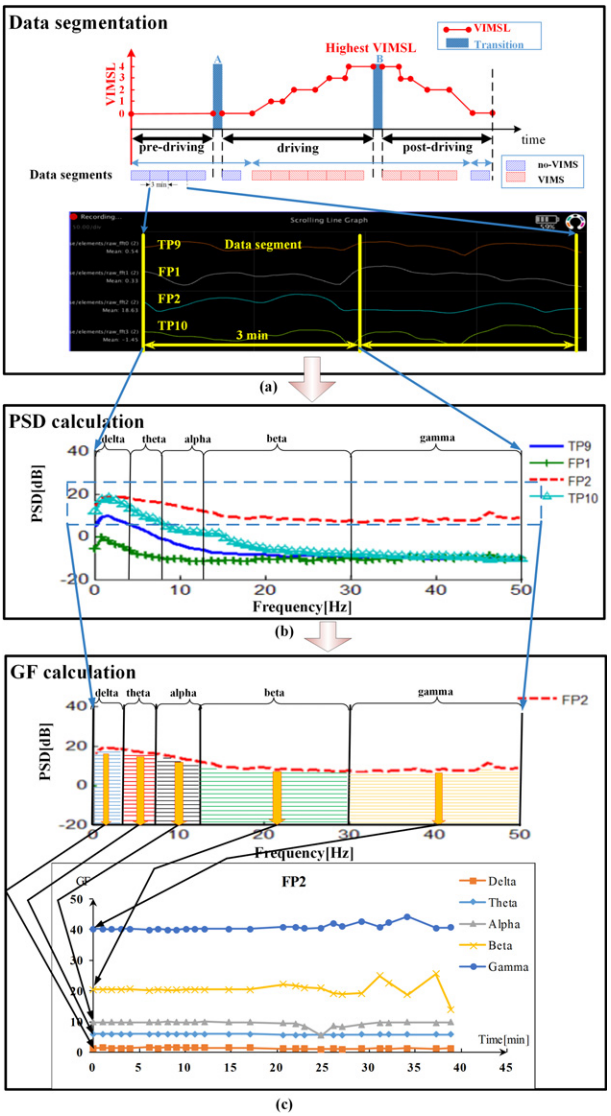

Figure 3. Flowchart of the gravity frequency (GF) computation. (a) The raw EEG data are segmented into 3-minute data segments. All the blue blocks (no-VIMS) and the red blocks (VIMS) in (a) are grouped by the states and their statistical features are calculated for comparisons of the two states. Data segmentation was done from the beginning of the experiment. This operation repeated until it meets the transitions of the action or the moments of change between no-VIMS and VIMS states. In general, segments less than three minutes are discarded. (b) The power spectral density (PSD) function for each data segment is computed for each electrode. Note that the PSD computation transforms each data segment in the temporal domain to the frequency domain. Therefore, we can separate the brain activity in each frequency band (alpha, beta, delta, ...). (c) The representative "center of mass" frequency of a given frequency range, GF, for each frequency band is calculated using Eq. (1) for each electrode. Note that GF computation brings the brain activity of each frequency band back to the temporal domain so that we can monitor the frequency bandwise activity monitoring in time. For the purpose of illustration, only GFs of FP2 are shown in the bottom figure.

each frequency band since Miyazaki et al. suggested that asynchronous bilateral MT+ activation (i.e., between two hemispheric brain areas) could be a marker of VIMS [6].

2.5.2 *Power Spectral Entropy*

Power spectral entropy is a measure of complexity reflecting the disorder of time sequence signals and the level of irregularity of multifrequency components signals [42]. The lower the PSE the more uniform the signal energy distribution over the whole frequency band [42]. Note that the PSE also has been shown as a sensitive parameter of brain activity classification in brain–computer interaction (e.g., imaginary hand movements) [55, 56]. The PSE is good for the measurement of nonlinear dynamic states, which requires a small amount of data [56]. The previous study has shown that the PSE can be used to distinguish different mental tasks (e.g., imagining that the left or right hand is moving) [56].

The Shannon entropy of the power spectrum of the signal can be defined as [42]

$$\mathrm{PSE} = -\sum_{f=f_1}^{f_2} p\left(f\right) \log_2 \left(p\left(f\right)\right), \tag{2}$$

where the probability of power occurrence for a given frequency, $p(f)$, can be computed as follows:

$$p\left(f\right) = \frac{PSD\left(f\right)}{\sum_{f=f_1}^{f_2} PSD\left(f\right)}, \quad f_1 \leq f \leq f_2. \tag{3}$$

Unlike the GF computation, PSE was computed to monitor the overall brain activities over the full frequency range within a given time range. So, we set $f_1 = 0$ Hz and $f_2 = 50$ Hz for Eq. (2) and Eq. (3), and PSE was computed for each electrode every 3-minute data segment.

2.5.3 *Kolmogorov Complexity (KC)*

Kolmogorov complexity can also be used to quantify the complexity of EEG signals [44]. Note that unlike the PSE, the KC measures the signal complexity directly from the *time domain* and not from the frequency domain. The KC has been used to measure the mental fatigue and showed encouraging results, where the KC of the EEG decreases as the mental fatigue increases (i.e., signal became less random when a person is in a mental fatigue state) [57].

KC computation consists of two steps: binary encoding and compression ratio computation. The temporal signals from each electrode were first encoded into a binary string (*symbol sequence*). A set of unique *binary words*, which could be concatenated to describe the full string, were identified, and then, the shortest length *binary word sequence* composed of a set of unique binary words were computed. Finally, the ratio of the shortest length (compressed) of the binary word sequence and the binary encoded string length (uncompressed) was computed and used for a measure of the signal complexity [58]. In other words, the KC is a maximum compression ratio of a signal when the signal is encoded into a binary code.

In our KC computation, the same 3-minute data segments used for GF and PSE computations were supplied to the encoding process. For each data segment, the raw EEG data were converted into a binary symbol sequence, $x =< x_0,$

Table II. Highest VIMSL that each subject experienced (L_{max}).

Subject	S1	S2	S3	S4	S5	S6	S7	S8
L_{max}	4	4	2	2	4	3	3	2

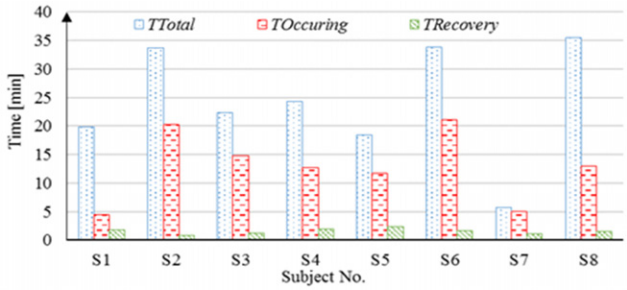

Figure 4. Comparison of the durations (T_{Total}, $T_{Occuring}$, and $T_{Recovery}$) between different subjects.

$x_1, x_2, \ldots, x_i, \ldots, x_{n-1} < (0 \le i \le n-1)$ using the following equation:

$$x_i = \begin{cases} 0 & x_i < \overline{x} \\ 1 & x_i \ge \overline{x}, \end{cases} \tag{4}$$

where

$$\overline{x} = \frac{1}{n} \sum_{i=0}^{n-1} x_i. \tag{5}$$

For each data segment, the complexity of the symbol sequence x of length n, KC, was obtained by

$$KC = \frac{c(n)}{b(n)}, \tag{6}$$

where $c(n)$ is the length of word sequence after the compression of the binary encoded input length of n, $b(n)$ reflects the length of word sequence before the compression, and $b(n) = \lim_{n\to\infty} c(n) \cong \frac{n}{\log_2 n}$ [44, 59]. Note that the KC varies within 0 and 1, where $KC = 1$ indicates the randomness of the signal reaching the maximum [45]. Similar to PSE, KC was computed for each electrode.

3. RESULTS AND DISCUSSIONS

3.1 *Subjective VIMSL Changes Analysis*

Let L_{max} be the highest VIMSL that the subject experienced, T_{Total} be the total driving duration, $T_{Occuring}$ be the length of time from the start of the drive to the occurrence of VIMS (the driving duration needed for VIMSL reaching "1"), and $T_{Recovery}$ be the recovery duration (the length of time from the end of the drive to the VIMSL coming back to "0"). Table II and Figure 4 show the distribution of those factors for eight subjects indicating a large individual difference in tolerance, susceptibility, and recoverability.

From Table II and Fig. 4, we can find the following:

(1) The total driving duration varies among the subjects. Generally, larger T_{Total} indicates higher VIMS tolerance. The T_{Total} for S2, S6, and S8 are larger than 30 minutes. These subjects showed higher VIMS tolerance.

Table III. Pearson linear correlation coefficients between T_{Total}, $T_{Occuring}$, $T_{Recovery}$, and L_{max}. Correlation coefficient $|r| \in [0, 0.8]$ indicates a relative weak linear relationship here.

Variables	PLCCr
T_{Total}, $T_{Occuring}$	0.78
T_{Total}, $T_{Recovery}$	−0.10
T_{Total}, L_{max}	−0.15
$T_{Occuring}$, $T_{Recovery}$	−0.21
$T_{Occuring}$, L_{max}	−0.11
$T_{Recovery}$, L_{max}	0.09

Table IV. Results of multivariate logistic regression.

Dependent variable	Independent variables	P
L_{max}	T_{Total}, $T_{Occuring}$, $T_{Recovery}$	0.24
$T_{Recovery}$	T_{Total}, $T_{Occuring}$, L_{max}	0.96
$T_{Occuring}$	T_{Total}, $T_{Recovery}$, L_{max}	0.96
T_{Total}	$T_{Occuring}$, $T_{Recovery}$, L_{max}	0.96

(2) The variation in $T_{Occuring}$ indicates that each subject had a different VIMS susceptibility in our study. Generally, smaller $T_{Occuring}$ indicates that subjects were more likely to get VIMS in a shorter time. The $T_{Occuring}$ for S1 and S7 are no more than 5 minutes. They were sensitive to VIMS.

(3) The recovery time for each subject also varied a lot. To a certain extent, smaller $T_{Recovery}$ indicates faster VIMS recoverability. The $T_{Recovery}$ for S3 is less than 3 minutes. It may suggest that S3 has a fast VIMS recoverability. However, S3 could only reach the VIMS level "2". A possible reason for this phenomenon was that S3 had not been "pushed" enough to reach the highest VIMS level. Therefore, we divided each subject's $T_{Recovery}$ by their max VIMSL (L_{max}) to be fair on comparing among the subjects.

In addition, we investigated the linear relationships between T_{Total}, $T_{Occuring}$, $T_{Recovery}$, and L_{max}. *Pearson linear correlation coefficients* (PLCC) between them are calculated and presented in Table III, but no strong ($|r| \le 0.8$) linear relationship between these variables was found.

We applied *multivariate nonlinear regression* analysis to the factors (T_{Total}, $T_{Occuring}$, $T_{Recovery}$, and L_{max}). As shown in Table IV, the results are $P \ge 0.05$ for all cases, indicating that a multivariate logistic regression model is invalid.

We also tried other models such as polynomial regression model, but no significant correlation was found (all $P \ge 0.05$). This suggests that no functional relationship exists between T_{Total}, $T_{Occuring}$, $T_{Recovery}$, and L_{max}.

3.2 *Objective EEG Data Analysis*

We computed the means and standard deviations of the GF, PSE, and KC measured in no-VIMS (VIMSL < 1) and VIMS (VIMSL ≥ 1) states for the eight subjects. Before the main

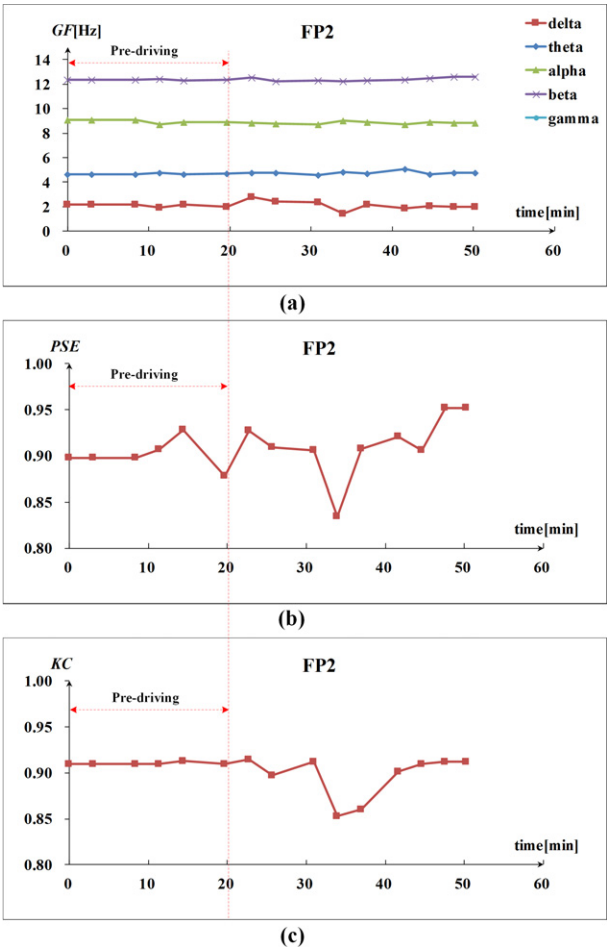

Figure 5. Temporal changes of the GF, PSE, and KC throughout the experiment. As an example, the figure shows the data from electrode FP2 of subject S1. (a) GF in five different frequency bands; (b) PSE; (c) KC.

analysis, we investigated whether those measures (GF, PSE, and KC) would vary simply as a function of time or not. If it turns out to be the case, we can hypothesize that those markers with significant differences between the two states, indeed, were caused by VIMS. Figure 5 shows the changes of GF, PSE, and KC of Subject S1 at FP2. From Fig. 5, we can see that there is no substantial variation for the potential EEG markers in the pre-driving segment. In this segment, no-VIMS occurred for all subjects. This indicates that GF, PSE, and KC may not vary over time without any VIMS. Therefore, it is reasonable for us to take the data of this segment as the baseline. Similar results can be obtained from the data from other subjects and electrodes.

In this section, scatterplots were used to show the changes of the means (standard deviations) of GF for each frequency band for all channels and the bilateral differences (FP2–FP1 and TP10–TP9). For PSE and KC, only the plots for all channels and the bilateral differences were generated. Each dot in the plots represents a subject's data. If there is a significant trend of increase or decrease due to the onset of VIMS, the majority of dots should be located above or below the diagonal line (i.e., no change), respectively. A pairwise

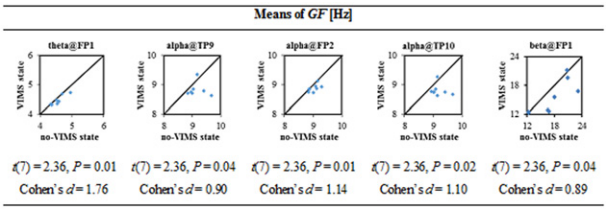

Figure 6. Comparison of the mean of GFs between no-VIMS state and VIMS state, which showed a significant difference ($P < 0.05$). The horizontal axis represents the mean GFs (Hz) in no-VIMS state, while the vertical axis represents the mean GFs (Hz) in VIMS state. Each dot in the plots represents a subject's data.

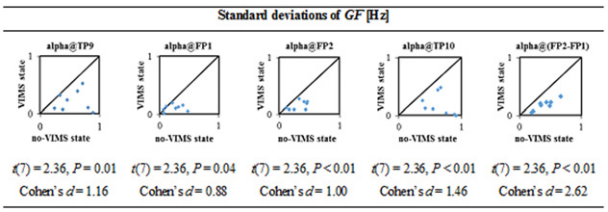

Figure 7. Comparison of the standard deviation of GFs between no-VIMS and VIMS states, which showed significant differences. The horizontal axis represents the standard deviation GFs (Hz) in no-VIMS state, while the vertical axis represents the standard deviation GFs (Hz) in VIMS state. Each dot in the plots represents a subject's data.

t-test was applied to find out whether the EEG markers were significantly different from no-VIMS state to VIMS state.

3.2.1 *Gravity Frequency*

Figure 6 shows the distributions of all mean GFs having significant changes ($P < 0.05$) between no-VIMS and VIMS states: theta@FP1, alpha@TP9, alpha@FP2, alpha@TP10, and beta@FP1. The P-value is corrected by Bonferroni correction. In these frequency bands and channels, the mean GFs in no-VIMS state are greater than those in VIMS state.

Similar analyses were carried out for the standard deviations of GFs for each frequency band for all channels. Figure 7 shows the results that are statistically significant ($P < 0.05$) between no-VIMS and VIMS states: alpha@TP9, alpha@FP1, alpha@FP2, alpha@TP10, and alpha@(FP2–FP1). In all cases, we can see that the standard deviations of GFs were increased in VIMS state, which indicates the decrease in the dispersion of the GFs during VIMS state. Note that all significant reductions of the dispersion were found in the alpha band.

The EEG power spectrums reflect fluctuations of the vigilant state [42] and are associated with various mental conditions [60]. For example, higher theta power is related to the increased activity in memory and attention processes, while higher beta power is associated with the spatial localization processes, and higher alpha power in the occipital lobe is associated with the level of relaxation [60].

In terms of VIMS, previous studies have shown that some EEG power-related measures will decrease after the onset of VIMS symptoms. Chen et al. argued that the overall decrease of the GF indicates the decline of subjects' alertness

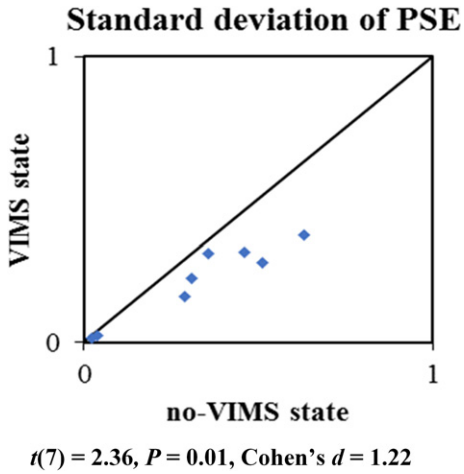

Figure 8. Scatterplot of the standard deviation of PSE for FP1. All data points are below the diagonal line, indicating the standard deviations of PSE for FP1 decreases when VIMS onset.

level [42], and especially, the alpha power suppression can be referred to the blocking or desynchronization of sensorimotor rhythms in parietal and the right and left motor areas of the brain, which might be influenced by vestibular inputs [29]. Naqvi et al. suspected that the drop in alpha power indicates the visual fatigue or discomfort caused by visual stimulus [41]. Our results are consistent with those literature. We suspect that the decrease of GF magnitude and variability might indicate the reduced mental activity and perceptual sensitivity in VIMS state.

We also noticed unusual signal noise in all bands and channels from time to time. We suspect that those might be caused by the poor connection between the electrodes and skin. However, since the GF worked as an average filter for the noise the impact of such signal noise was automatically reduced in GF analysis.

3.2.2 *Power Spectral Entropy*

As mentioned in the previous section, PSE is a sensitive brain activity classification parameter, reflecting the spectral structure of EEG signals [56]. Lower average PSE represents a uniform signal energy distribution over the whole frequency band, while lower standard deviations of PSE indicate a less disturbance or fluctuation in signal energy distribution.

Figure 8 shows the distribution of the standard deviation of PSE for FP1, which turned out to be the only measurement, showing a statistically significant ($t(7) = 2.36$, $P = 0.01$) difference between no-VIMS and VIMS states. As can be seen from the figure, all data points are located below the diagonal line, indicating that the standard deviations of PSE for FP1 in no-VIMS state were larger than that in VIMS state. We suspect that when VIMS occurred, the brain activity at FP1 was significantly suppressed (as also shown in GF analysis for alpha and theta wave of the FP1, Fig. 7). As a result, the signal energy distribution turned uniform, and the signal fluctuation decreased as well. No significant change of mean PSE was observed for VIMS onset.

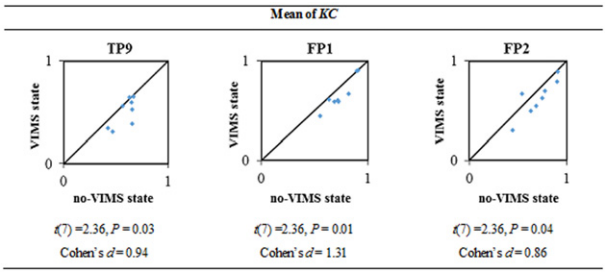

Figure 9. Comparison of the means of KC for the signal channels (electrodes) which showed significant differences between no-VIMS and VIMS states.

3.2.3 *Kolmogorov Complexity*

As it can be seen in Figure 9, the means of KC for EEG signals collected from all electrodes, except from TP10, showed a significant decrease (all $P < 0.05$) with the onset of VIMS.

Previous studies have shown that KC of the EEG signal is strongly correlative with mental fatigue [44, 57]. They found that the KC decreases as mental fatigue increases [44, 57]. In addition, Gao et al. found that the KC sharply drops shortly after the epileptic seizure. They showed that the transient EEG signals associated with epileptic seizures contain less random components than normal background EEGs [58]. All these studies showed that KC values would decrease when brain activity changes from normal to abnormal. Our results also supported similar trends such that a decrease of KC occurred with VIMS onset. We suspect that when VIMS occurred, brain activity was significantly suppressed and caused a decrease of KC.

4. CONCLUSIONS

The purpose of this pilot study was to analyze the relationship between the EEG and subjective VIMS rating and find possible EEG markers for VIMS evaluation. An EEG device with four electrodes was used to collect data. We computed the mean and standard deviation of various EEG signal descriptors and compared the values between no-VIMS and VIMS states in an attempt to differentiate whether a subject was in no-VIMS or VIMS state based on those signal descriptors.

Our studies suggest the following:

(1) The tolerance, susceptibility, and recoverability of a subject to VIMS were quite different between subjects. It seems there was no functional relationship between each subject's tolerance, susceptibility, recoverability, and subjectively rated VIMS level.

(2) For the following frequency bands and channels of EEG, the means of GF decreased significantly in VIMS state: theta@FP1, alpha@TP9, alpha@FP2, alpha@TP10, and beta@FP1.

(3) For the following frequency bands and channels of EEG, the standard deviations of GF, which indicates the dispersion of the brain signal, decreased significantly in VIMS state: alpha@TP9, alpha@FP1, alpha@FP2, alpha@TP10, and alpha@(FP2–FP1).

(4) A significant reduction of the standard deviation of PSE was observed at FP1 when VIMS occurred.
(5) There was a significant reduction in the means of KC for TP9, FP1, and FP2 when VIMS occurred.
(6) The values of Cohen's d for each of the *statistically significant t-tests* were large ($d > 0.80$), indicating that the EEG markers that we identified are indeed strong indicators of VIMS.
(7) An EEG device with a small number of electrodes (four electrodes) is feasible to perform VIMS evaluation.

All the identified markers showed a decrease after the onset of VIMS. This may represent our brain's physiological response to VIMS. Note that the physiological markers presented by some other studies also showed decreases after the occurrence of VIMS [17, 42]. They suspected that it may be caused by the decline of subjects' alertness level [42] or depressed brain activity [44, 57].

Although we found significant differences between no-VIMS and VIMS states, it is hard to conclude that these markers can be directly used for precise detection of VIMS onset or estimation of VIMS severity in real time, because our analyses focused only on differences occurred between no-VIMS and VIMS states.

In addition, changes in these markers are not a necessary and sufficient condition for VIMS occurrence. This is because some VIMS-like symptoms that occur in certain situations may be related to factors other than VIMS ("various mental conditions"), or even have nothing to do with VIMS [61].

Furthermore, we do not know the exact physiological mechanism of GF, PSE, and KC changes to the VIMS level scoring. For example, Wei et al. have shown that changes in the alertness level were monotonically related to changes in the EEG power spectrum in the theta and alpha bands [62]; Lin et al. have shown that the improved behavioral performance was accompanied by concurrent power suppression in the theta and alpha bands in the occipital cortices [63]. Thus, more evidence is needed to confirm the causality of EEG markers.

In current study paradigm, it is difficult to determine if the measured EEG signal difference is contaminated by the emotional or physical impact of the task (e.g., driving) or truly by the onset of VIMS. Therefore, our results should be verified further in a more controlled experimental design where only passive visual stimulation is provided.

Finally, to make the finding more useful, further analysis should be developed to enable detection of VIMS onset and estimation of VIMS level in real time. Currently, we are working on designing a machine-learning approach to handle such a task.

ACKNOWLEDGMENT

This work was supported by the Google Faculty Research Awards, the Fundamental Research Funds for the Central Universities (2018CDXYJSJ0026, 2019CDYGZD004), the NIH P30 core grant (P30EY003790), the Science and Technology Innovation Project for Young Scholars of SXAU (2018024), the Chongqing Foundation & Advanced Research Project (cstc2019jcyj-msxmX0622), the Entrepreneurship and Innovation Program for Chongqing Overseas Returned Scholars (No. cx2017094), and the Science and Technology Research Program of Chongqing Municipal Education Commission (No. KJQN201800111). The funders had no role in study design, data collection and analysis, decision to publish, or preparation of the manuscript. The authors thank the volunteers who participated in the experiment.

REFERENCES

[1] A. Jarvinen, "Virtual reality as trend contextualising an emerging consumer technology into trend analysis," *Future Technologies Conference* (Institute of Electrical and Electronics Engineers Inc., San Francisco, CA, 2016), pp. 1065–1070.
[2] A. S. Fernandes and S. K. Feiner, "Combating VR sickness through subtle dynamic field-of-view modification," *IEEE Symposium on 3D User Interfaces* (IEEE, Piscataway, NJ, 2016), pp. 201–210.
[3] L. J. Hettinger and G. E. Riccio, "Visually induced motion sickness in virtual environments," Presence Teleoperators Virtual Environments **1**, 306–310 (1992).
[4] R. S. Kennedy, J. Drexler, and R. C. Kennedy, "Research in visually induced motion sickness," Appl. Ergon. **41**, 494–503 (2010).
[5] S. Ohyama, S. Nishiike, H. Watanabe, K. Matsuoka, H. Akizuki, N. Takeda, and T. Harada, "Autonomic responses during motion sickness induced by virtual reality," Auris Nasus Larynx **34**, 303–306 (2007).
[6] J. Miyazaki, H. Yamamoto, Y. Ichimura, H. Yamashiro, T. Murase, T. Yamamoto, M. Umeda, and T. Higuchi, "Inter-hemispheric desynchronization of the human MT+ during visually induced motion sickness," Exp. Brain Res. 2421–2431 (2015).
[7] A. D. Hwang and E. Peli, "Instability of the perceived world while watching 3D stereoscopic imagery: A likely source of motion sickness symptoms," i-Perception **5**, 515–535 (2014).
[8] S. Classen, M. Bewernitz, and O. Shechtman, "Driving simulator sickness: An evidence-based review of the literature," Am. J. Occup. Ther. **65**, 179–188 (2011).
[9] C. T. Lin, S. F. Tsai, and L. W. Ko, "EEG-based learning system for online motion sickness level estimation in a dynamic vehicle environment," IEEE Trans. Neural Netw. Learn. Syst **24**, 1689–1700 (2013).
[10] R. S. Kennedy, N. E. Lane, K. S. Berbaum, and M. G. Lilienthal, "Simulator sickness questionnaire: An enhanced method for quantifying simulator sickness," Int. J. Aviat. Psychol. **3**, 203–220 (1993).
[11] B. Keshavarz and H. Hecht, "Validating an efficient method to quantify motion sickness," Hum. Factors **53**, 415–426 (2011).
[12] B. Cheung and P. Vaitkus, "Perspectives of electrogastrography and motion sickness," Brain Res. Bull. **47**, 421–431 (1998).
[13] H. Ujike and H. Watanabe, "Effects of stereoscopic presentation on visually induced motion sickness," Proc. SPIE **7863** (2011).
[14] O. D. Kothgassner, A. Felnhofer, H. Hlavacs, L. Beutl, R. Palme, I. Kryspin-Exner, and L. M. Glenk, "Salivary cortisol and cardiovascular reactivity to a public speaking task in a virtual and real-life environment," Comput. Hum. Behav. **62**, 124–135 (2016).
[15] S. D. Norrholm, T. Jovanovic, M. Gerardi, K. G. Breazeale, M. Price, M. Davis, E. Duncan, K. J. Ressler, B. Bradley, and A. Rizzo, "Baseline psychophysiological and cortisol reactivity as a predictor of PTSD treatment outcome in virtual reality exposure therapy," Behav. Res. Ther. **82**, 28–37 (2016).
[16] N. Sugita, M. Yoshizawa, A. Tanaka, K. Abe, S. Chiba, T. Yambe, and S.-i. Nitta, "Quantitative evaluation of effects of visually-induced motion sickness based on causal coherence functions between blood pressure and heart rate," Displays **29**, 167–175 (2008).
[17] S. A. A. Naqvi, N. Badruddin, M. A. Jatoi, A. S. Malik, W. Hazabbah, and B. Abdullah, "EEG based time and frequency dynamics analysis of visually induced motion sickness (VIMS)," Australas. Phys. Eng. Sci. Med. **38**, 721–729 (2015).
[18] L. W. Ko, H. C. Lee, S. F. Tsai, T. C. Shih, Y. T. Chuang, H. L. Huang, S. Y. Ho, and C. T. Lin, "EEG-based motion sickness classification system with genetic feature selection," *IEEE Symposium on Computational Intelligence,*

Cognitive Algorithms, Mind, and Brain (IEEE, Piscataway, NJ, 2013), pp. 158–164.
[19] F. Koslucher, E. Haaland, and T. A. Stoffregen, "Sex differences in visual performance and postural sway precede sex differences in visually induced motion sickness," Exp. Brain Res. **234**, 313–322 (2016).
[20] S. A. Nooij, P. Pretto, D. Oberfeld, H. Hecht, and H. H. Bülthoff, "Vection is the main contributor to motion sickness induced by visual yaw rotation: Implications for conflict and eye movement theories," Plos One **12**, e0175305 (2017).
[21] C. C. T. Guo, D. J. Z. Chen, I. Y. Wei, R. H. Y. So, and R. T. F. Cheung, "Correlations between individual susceptibility to visually induced motion sickness and decaying time constant of after-nystagmus," Appl. Ergon. **63**, 1–8 (2017).
[22] W. Bles, J. E. Bos, B. d. Graaf, E. Groen, and A. H. Wertheim, "Motion sickness: only one provocative conflict?," Brain Res. Bull. **47**, 481–487 (1998).
[23] J. T. Reason, "Motion sickness adaptation: A neural mismatch model," J. R. Soc. Med. **71**, 819–829 (1978).
[24] H. Takada, K. Fujikake, T. Watanabe, S. Hasegawa, M. Omori, and M. Miyao, "A method for evaluating motion sickness induced by watching stereoscopic images on a head-mounted display," Proc. SPIE **7237**, 72371P-1–72371P-8 (2009).
[25] C. T. Lin, S. F. Tsai, H. C. Lee, H. L. Huang, S. Y. Ho, and L. W. Ko, "Motion sickness estimation system," *Int'l. Joint Conf. on Neural Networks* (Institute of Electrical and Electronics Engineers Inc., Brisbane, QLD, Australia, 2012).
[26] C. S. Wei, L. W. Ko, S. W. Chuang, T. P. Jung, and C. T. Lin, "EEG-based evaluation system for motion sickness estimation," *5th Int'l. IEEE/EMBS Conference on Neural Engineering* (IEEE, Piscataway, NJ, 2011), pp. 100–103.
[27] C. S. Wei, S. W. Chuang, W. R. Wang, L. W. Ko, T. P. Jung, and C. T. Lin, "Implementation of a motion sickness evaluation system based on EEG spectrum analysis," *IEEE Int'l. Symposium of Circuits and Systems* (IEEE, Piscataway, NJ, 2011), pp. 1081–1084.
[28] Y. C. Chen, J. R. Duann, S. W. Chuang, C. L. Lin, L. W. Ko, T. P. Jung, and C. T. Lin, "Spatial and temporal EEG dynamics of motion sickness," NeuroImage **49**, 2862–2870 (2010).
[29] Y. C. Chen, J. R. Duann, C. L. Lin, S. W. Chuang, T. P. Jung, and C. T. Lin, "Motion-sickness related brain areas and EEG power activates," *5th Int'l Conf. on Foundation of Augmented Cognition*, edited by D. D. Schmorrow, I. V. Estabrooke, and M. Grootjen (Springer, Berlin, 2009), pp. 348–354.
[30] G. E. Riccio and T. A. Stoffregen, "An ecological theory of motion sickness and postural instability," Ecological Psychol. **3**, 195–240 (1991).
[31] C. H. Chang, W. W. Pan, L. Y. Tseng, and T. A. Stoffregen, "Postural activity and motion sickness during video game play in children and adults," Exp. Brain Res. **217**, 299–309 (2012).
[32] C. H. Chang, W. W. Pan, F. C. Chen, and T. A. Stoffregen, "Console video games, postural activity, and motion sickness during passive restraint," Exp. Brain Res. **229**, 235–242 (2013).
[33] T. A. Stoffregen and L. J. S. Jr, "Postural instability precedes motion sickness," Brain Res. Bull. **47**, 437–448 (1998).
[34] S. M. Ebenholtz, M. M. Cohen, and B. J. Linder, "The possible role of nystagmus in motion sickness: A hypothesis," Aviat. Space Environ. Med. **65**, 1032–1035 (1994).
[35] S. Hu and R. M. Stern, "Optokinetic nystagmus correlates with severity of vection-induced motion sickness and gastric tachyarrhythmia," Aviat. Space Environ. Med. **69**, 1162–1165 (1998).
[36] J. T. T. Ji, R. H. Y. So, and R. T. F. Cheung, "Isolating the effects of vection and optokinetic nystagmus on optokinetic rotation-induced motion sickness," Hum. Factors **51**, 739–751 (2009).
[37] J. Dichgans and T. Brandt, "Optokinetic motion sickness and pseudo-Coriolis effects induced by moving visual stimuli," Acta Oto-Laryngologica **76**, 339–348 (1973).
[38] M. Polonen and J. Hakkinen, "Near-to-eye display—An accessory for handheld multimedia devices: Subjective studies," J. Disp. Technol. **5**, 358–367 (2009).
[39] J. R. Lackner, "Motion sickness: more than nausea and vomiting," Exp. Brain Res. **232**, 2493–2510 (2014).
[40] C. T. Lin, S. W. Chuang, Y. C. Chen, L. W. Ko, S. F. Liang, and T. P. Jung, "EEG effects of motion sickness induced in a dynamic virtual reality environment," *29th Annual Int'l. Conf. IEEE Engineering in Medicine and Biology Society* (IEEE, Piscataway, NJ, 2007), pp. 3872–3875.
[41] S. A. A. Naqvi, N. Badruddin, A. S. Malik, W. Hazabbah, and B. Abdullah, "EEG alpha power: An indicator of visual fatigue," *5th Int'l. Conf. on Intelligent and Advanced Systems* (IEEE, Piscataway, NJ, 2014).
[42] C. Chen, J. Wang, K. Li, Q. Wu, H. Wang, Z. Qian, and N. Gu, "Assessment visual fatigue of watching 3DTV using EEG power spectral parameters," Displays **35**, 266–272 (2014).
[43] X. Wang, Z. Qian, L. Xing, S. Jin, B. Liu, Z. Li, and J. Yin, "The study of human health effect induced by depth information of stereo vision film," J. Innovative Opt. Health Sci. **8**, 23–28 (2015).
[44] J. Liu, C. Zhang, and C. Zheng, "EEG-based estimation of mental fatigue by using KPCA-HMM and complexity parameters," Biomed. Signal Process. Control **5**, 124–130 (2010).
[45] X. M. Pei, C. X. Zheng, W. X. He, and J. Xu, "Quantitative measure of complexity of the dynamic event-related EEG data," Neurocomputing **70**, 263–272 (2006).
[46] H. S. Cai, Y. F. Chen, J. S. Han, X. Z. Zhang, and B. Hu, "Study on feature selection methods for depression detection using three-electrode EEG data," Interdiscip. Sci. **10**, 558–565 (2018).
[47] R. Liu, E. Peli, and A. D. Hwang, "Measuring visually induced motion sickness using wearable devices," *IS&T Electronic Imaging: Human Vision and Electronic Imaging 2017* (IS&T, Springfield, VA, 2017), pp. 218–223.
[48] M. A. Lopez-Gordo, D. S. Morillo, and F. P. Valle, "Dry EEG electrodes," Sensors (Switzerland) **14**, 12847–12870 (2014).
[49] T. J. Sullivan, S. R. Deiss, T.-P. Jung, and G. Cauwenberghs, "A brain-machine interface using dry-contact, low-noise EEG sensors," *IEEE Int'l. Symposium on Circuits and Systems* (IEEE, Piscataway, NJ, 2008), pp. 1986–1989.
[50] X. Zhou, Q. Li, S. Kilsgaard, F. Moradi, S. L. Kappel, and P. Kidmose, "A wearable ear-EEG recording system based on dry-contact active electrodes," *30th IEEE Symposium on VLSI Circuits* (IEEE, Piscataway, NJ, 2016), pp. 1–2.
[51] S. D'Amour, J. E. Bos, and B. Keshavarz, "The efficacy of airflow and seat vibration on reducing visually induced motion sickness," Exp. Brain Res. **235**, 2811–2820 (2017).
[52] K. J. Hill and P. A. Howarth, "Habituation to the side effects of immersion in a virtual environment," Displays **21**, 25–30 (2000).
[53] B. Keshavarz, A. C. Novak, L. J. Hettinger, T. A. Stoffregen, and J. L. Campos, "Passive restraint reduces visually induced motion sickness in older adults," J. Exp. Psychol. Appl. **23**, 85–99 (2017).
[54] J. A.-A. Smither, M. Mouloua, and R. Kennedy, "Reducing symptoms of visually induced motion sickness through perceptual training," Int. J. Aviat. Psychol. **18**, 326–339 (2008).
[55] K. M. Wang, N. Zhong, and H. Y. Zhou, "Activity analysis of depression electroencephalogram based on modified power spectral entropy," Acta Phys. Sin. **63**, 533–538 (2014).
[56] A. Zhang, B. Yang, and L. Huang, "Feature extraction of EEG signals using power spectral entropy," *Int'l. Conf. on BioMedical Engineering and Informatics* (IEEE, Piscataway, NJ, 2008), pp. 435–439.
[57] L. Y. Zhang and C. X. Zheng, "Analysis of Kolmogorov complexity in spontaneous EEG signal and it's application to assessment of mental fatigue," *2nd Int'l. Conf. on Bioinformatics and Biomedical Engineering* (IEEE, Piscataway, NJ, 2008), pp. 2192–2194.
[58] J. Gao, J. Hu, and W. W. Tung, "Complexity measures of brain wave dynamics," Cogn. Neurodynamics **5**, 171–182 (2011).
[59] D. Labate, F. L. Foresta, G. Morabito, I. Palamara, and F. C. Morabito, "Entropic measures of EEG complexity in alzheimer's disease through a multivariate multiscale approach," IEEE Sensors J. **13**, 3284–3292 (2013).
[60] A. S. Malik, R. N. H. R. Khairuddin, H. U. Amin, M. L. Smith, N. Kamel, J. M. Abdullah, S. M. Fawzy, and S. Shim, "EEG based evaluation of stereoscopic 3D displays for viewer discomfort," Biomed. Eng. Online **14**, 21 (2015).
[61] K. Stanney, G. Salvendy, J. Deisinger, P. Dizio, S. Ellis, J. Ellison, G. Fogleman, J. Gallimore, M. Singer, L. Hettinger, R. Kennedy, J. Lackner, B. Lawson, J. Maida, A. Mead, M. Mon-Williams, D. Newman, T. Piantanida, L. Reeves, O. Riedel, T. Stoffregen, J. Wann, R. Welch, J. Wilson, and B. Witmer, "Aftereffects and sense of presence in virtual environments: Formulation of a research and development agenda," Int. J. Hum.-Comput. Interact. **10**, 135–187 (1998).
[62] C. S. Wei, L. W. Ko, S. W. Chuang, T. P. Jung, and C. T. Lin, "Genetic feature selection in EEG-based motion sickness estimation," *Int'l. Joint Conf. on Neural Network* (IEEE, Piscataway, NJ, 2011), pp. 365–369.
[63] C. T. Lin, K. C. Huang, C. F. Chao, J. A. Chen, T. W. Chiu, L. W. Ko, and T. P. Jung, "Tonic and phasic EEG and behavioral changes induced by arousing feedback," Neuroimage **52**, 633–642 (2010).